

pubs.acs.org/JACS Article

Core-Shell Gyroid in ABC Bottlebrush Block Terpolymers

Shuquan Cui, Bo Zhang, Liyang Shen, Frank S. Bates,* and Timothy P. Lodge*



Cite This: J. Am. Chem. Soc. 2022, 144, 21719–21727



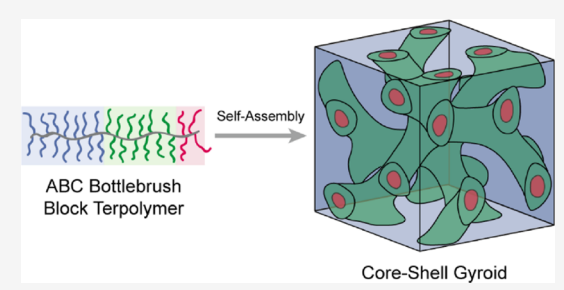
ACCESS

Metrics & More

Article Recommendations

Supporting Information

ABSTRACT: Block polymer self-assembly provides a versatile platform for creating useful materials endowed with three-dimensional periodic network morphologies that support orthogonal physical properties such as high ionic conductivity and a high elastic modulus. However, coil configurations limit conventional linear block polymers to finite ordered network dimensions, which are further restricted by slow self-assembly kinetics at high molecular weights. A bottlebrush architecture can circumvent both shortcomings owing to extended backbone configurations due to side chain crowding and molecular dynamics substantially free of chain entanglements. However, until now, network morphologies have not been reported in AB bottlebrush block



copolymers, notwith standing favorable mean-field predictions. We explored the phase behavior by small-angle X-ray scattering of 133 poly(ethylene-alt-propylene)-b-polystyrene (PEP-PS) diblock and PEP-PS-PEO triblock bottle brush copolymers prepared by ring-opening metathesis polymerization (ROMP) of nor bornene-functionalized poly(ethylene-alt-propylene) (PEP), poly (PS), and poly(ethylene oxide) (PEO) macromonomers with total backbone degrees of polymerization (PEP-PS diblocks exhibited only cylindrical and lamellar morphologies over the composition range of ca. 30–70%. However, addition of variable-length bottle brush PEO blocks to diblocks containing 30–50% PS led to the formation of a substantial core–shell double gyroid (GYR) phase window containing 20 bottle brush triblock specimens, which is the focus of this report. Encouragingly, the GYR unit cell dimensions increased as $d \sim N_{\rm bb}^{0.92}$, portending the ability to access larger network dimensions than previously obtained with linear AB or ABC block polymers. This work highlights extraordinary opportunities associated with applying facile ROMP chemistry to multiblock bottle brush polymers.

■ INTRODUCTION

Network materials with interpenetrating nanodomains have attracted significant interest because of their unique properties, ^{1,2} affording a versatile tool for numerous applications, from ion transport media, ³ nanoporous membranes, ⁴ therapeutic delivery vehicles, ⁵ templated mesoporous inorganic materials, ^{6–8} to large-scale photonics and metamaterials. ^{9,10} The desired pore diameter may range from several nanometers to above 100 nm. Compared with time-consuming top-down strategies such as lithography, which is limited in material size, ¹ the self-assembly of block copolymers may be considered a facile bottom-up path for network preparation.

The self-assembly of block copolymers originates from a balance of the interfacial energy penalty versus the entropic cost of chain stretching. 11,12 For linear AB diblock copolymers, phase behavior is mainly determined by the segregation strength (parameterized by the product of the volumetric degree of polymerization N and the Flory–Huggins segment–segment interaction parameter χ) and the volume fraction of one block type f. The evolution of periodic nanostructures with the sequence of S-HEX-network-LAM-network-HEX-S with f is usually observed in a classic phase portrait of linear diblocks, where S, HEX, and LAM denote spherical, hexagonally packed cylindrical, and lamellar morphologies, respectively. 16 Thermodynamically stable network phases

found in linear diblocks include double gyroid (GYR, Q²³⁰) and orthorhombic *Fddd* (O⁷⁰).¹⁷

One of the principal obstacles to the application of selfassembled block polymer-based networks is access to a limited pore diameter or unit cell dimension (usually <50 nm). $^{18-20}$ The dimension d of self-assembled morphologies derived from flexible linear blocks, governed by Gaussian statistics in the unperturbed state, depends mainly on the copolymer molecular weight (MW), $d \sim N^{2/3.15}$ At high molecular weight, such scaling is accompanied by entanglements, which significantly slow down self-assembly kinetics,²¹ detrimental to the formation of well-ordered networks. Additionally, compared with other phases such as LAM and HEX, the network composition window of linear diblocks is very narrow (the range of f is often below 0.05),²² further increasing the difficulties of accessing large domain networks. Scaling up network dimensions in block copolymers remains a daunting challenge and important for both academia and industry.

Received: September 9, 2022 Published: November 15, 2022





Scheme 1. Synthesis Route to Bottlebrush Di- and Triblock Polymers

"PEP-PS diblock bottlebrush copolymers were obtained by terminating 4 using ethyl vinyl ether to remove the terminal catalyst group [Ru]; the same termination procedure was also used for the PEP-PS-PEO triblock bottlebrush copolymers 6.

Bottlebrush polymers consisting of densely grafted side chains along a central backbone have become an attractive focus based on their distinctive properties compared to linear counterparts.^{23,24} The kinetics of bottlebrush ordering can be much faster than that of linear polymers because the high entanglement density that hinders ordering in high MW linear polymer melts is generally absent in bottlebrush polymers, due to the large macromolecular cross-sectional area.²⁵ Compared with other bottlebrush polymers, such as Janus bottlebrushes, gradient bottlebrushes, and core-shell bottlebrushes, the bottlebrush block polymer is more promising for achieving large domain spacings, as the domain spacing strongly couples to the central backbone degree of polymerization with an exponent of 0.8-0.9, larger than the 0.5-0.67 typical of linear systems. 26 Xia et al. compared the lamellar domain spacing of bottlebrush copolymers with different side chain arrangements while fixing other parameters. The domain spacing of block bottlebrushes (116 nm) was significantly larger than that of random bottlebrushes (14 nm).²⁷ Other studies also showed that domain spacings of block bottlebrushes up to several hundred nanometers could be achieved. 21,28 Numerous studies have documented several different morphologies in block bottlebrushes. However, the relatively stiff molecular structure of bottlebrush block polymers is best accommodated by flat domain interfaces, that is, lamellar morphologies, even for systems with highly asymmetric volume fractions.²⁹ To realize a HEX phase with curved interfaces, the introduction of architectural asymmetry (i.e., asymmetry in side chain length) has proven to be an effective approach. 30 Using self-consistent field theory (SCFT), Park et al. established the thermodynamic stability of the GYR phase in bottlebrush diblock copolymer melts.³¹ Meanwhile, Lequieu et al. predicted the existence of the alternating gyroid (Q214) and the alternating diamond network phases in ABC triblock bottlebrush terpolymers.³² Nevertheless, to date, no network phase has been experimentally found in diblock bottlebrush copolymers, while a few groups reported network phases (GYR) in other bottlebrush architectures, such as Janus bottlebrushes, 33 gradient bottlebrushes,³⁴ and linear-bottlebrush copolymers.^{35,36} Realizing the network phase in block bottlebrush copolymers should pave the way to larger dimension networks.

In this study, we systematically explore the phase behavior of both AB diblock and ABC triblock bottlebrush block polymers experimentally. A combination of anionic polymerization and ring-opening metathesis polymerization (ROMP, Scheme 1) enabled the efficient and controllable synthesis of 133

bottlebrush block polymers, providing a host of materials for the investigation of phase behavior. This report focuses primarily on a subset of 20 bottlebrush triblock copolymers that form a core-shell GYR network morphology. The chosen chemistries are poly(ethylene-alt-propylene)-b-polystyrene (PEP-PS) diblock and poly(ethylene-alt-propylene)-b-polystyrene-b-poly(ethylene oxide) (PEP-PS-PEO) triblock bottlebrush block polymers. Anticipating that network phases are most likely to appear in the low-MW region,³⁷ we designed the bottlebrush copolymers with relatively short side chains and short backbone degrees of polymerization. A core-shell GYR network phase was realized for the first time with a substantial subset of these block bottlebrush copolymers. These findings provide a springboard for creating network phases in block bottlebrush copolymers, enabling the pursuit of various applications that require control over copolymer self-assembly across a wide range of length scales.

RESULTS

Synthesis and Characterization of Bottlebrush Block Copolymers. PEP-PS diblock and PEP-PS-PEO triblock bottlebrush polymers were synthesized by sequential ROMP using the Grubbs 3rd (G3) catalyst, as outlined in Scheme 1. ROMP is an efficient and controllable approach and affords accurate molecular weight and composition control based on the molar ratio of each macromonomer added to the G3 catalyst, with concurrent very low molar-mass dispersity (D). 38,39 Macromonomers of PEP (MM_P), PS (MM_S), and PEO (MM_O) with D < 1.15 were synthesized by esterification of exo-5-norbornenecarboxylic acid and hydroxy precursors from anionic polymerization (ω -hydroxyl PEP and ω -hydroxyl PS) or purchased from commercial suppliers (PEO monomethyl ether). The detailed synthetic procedures and molecular characterization are provided in the Supporting Information (Schemes S1-S5 and Figures S1-S6).

Proton nuclear magnetic resonance (1 H NMR) spectra of MM_P, MM_S, and MM_O (Figure 1) indicated high purity for all three macromonomers and were employed to calculate the number-average MW (M_n) by end group analysis. The dispersity D was characterized by size-exclusion chromatography (SEC) with a refractive index (RI) detector using tetrahydrofuran (THF) as the eluent. Table 1 lists the molecular parameters of the macromonomers. The M_n of all macromonomers was maintained near 1 kg/mol, leading to bottlebrush blocks with almost symmetric architectures.

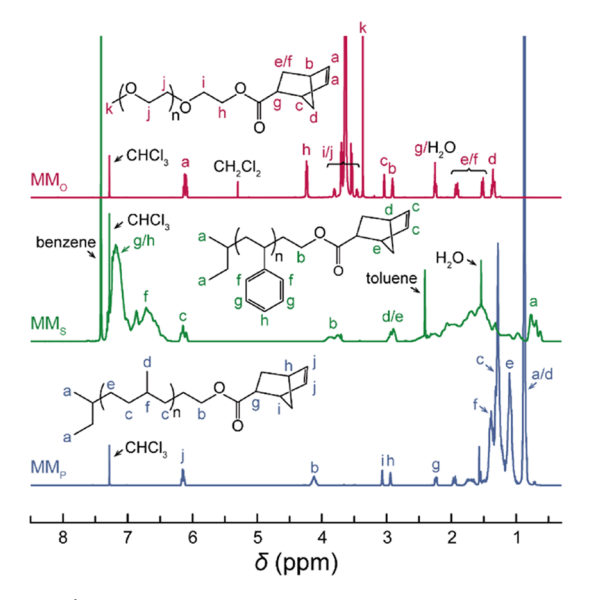


Figure 1. ¹H NMR spectra of MM_P, MM_S, and MM_O in CDCl₃.

Table 1. Macromonomer Parameters

ID	$M_{\rm n} (g/{\rm mol})^a$	D^{b}	DP^c
MM_P	1290	1.11	15.2
MM_S	1240	1.14	9.8
MM_O	1090	1.10	20.3

^aDetermined by end group analysis from ¹H NMR spectra. ^bDetermined by SEC with a RI detector using THF as the eluent. ^cAverage chemical degree of polymerization.

We employed a standard procedure (described in Supporting Information, Scheme S5) to controllably synthesize a variety of triblock PEP-PS-PEO terpolymers along the isopleth in the ternary phase portrait defined by constant $f_{\rm PEP}/f_{\rm PS}$ but different $f_{\rm PEO}$, where $f_{\rm PEP}, f_{\rm PS}$, and $f_{\rm PEO}$ represent the volume fraction of the PEP, PS, and PEO blocks, respectively. Polymers along a specific isopleth were obtained from a parent PEP-PS diblock ($f_{\rm PEO}=0.0$), which spawned several child PEP-PS-PEO triblocks with $f_{\rm PEO}>0.0$. Each bottlebrush SEC profile shown in Figure 2 contains a single narrow peak, associated with virtually complete reaction. Molecular parameters of all bottlebrush copolymers are provided in Tables S1 and S2. For convenience, the bottlebrush copolymers are identified as BB($f_{\rm PEP}/f_{\rm PS}, f_{\rm PEO}$).

Phase Behavior of PEP-PS Diblock Bottlebrush **Copolymers.** We first characterized the bulk phase behavior of PEP-PS diblock bottlebrush copolymers using small-angle X-ray scattering (SAXS), carried out either at the Advanced Photon Source (APS) at Argonne National Laboratory, Sector 12-ID-B beamline or at the Characterization Facility, University of Minnesota, using a Xenocs Ganesha instrument (Ganesha) equipped with a four-position heating stage (INSTEC). Prior to making SAXS measurements, the dried samples were annealed at 150 °C (well above the $T_{\rm g}$ of both blocks, see Figure S7) under vacuum for 48 h. Neither degradation nor cross-linking occurred according to SEC profiles obtained following the annealing process (Figure S8). (A weak RI response at long elution times (e.g., 16-17 min in Figure S6) is attributed to unreacted macromonomers (or linear homopolymer lacking a norbornene group), which amounts to <2% impurity.) Phase behavior was mainly

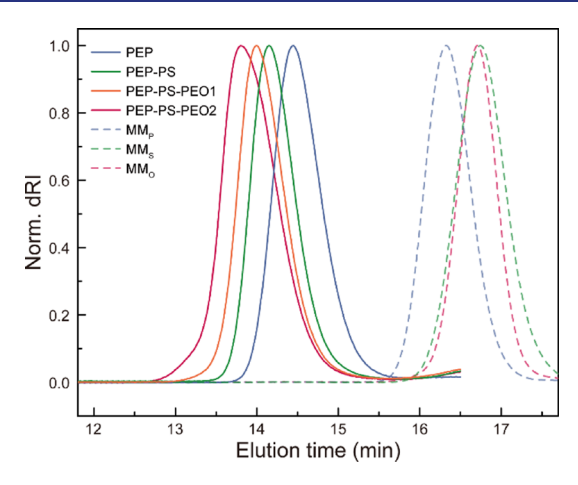


Figure 2. SEC profiles of bottlebrush polymers along with the corresponding macromonomers. Here, PEP, PEP-PS, and PEP-PS-PEO denote the bottlebrush homopolymer, the diblock bottlebrush copolymer, and the triblock bottlebrush polymer, respectively, and are from a single synthesized batch. PEP-PS-PEO1 and PEP-PS-PEO2 selected here are BB(1.00, 0.16) and BB(1.00, 0.37), respectively.

investigated at 140 °C, supplemented by some sample measurements at 80 °C. Figure 3 presents representative

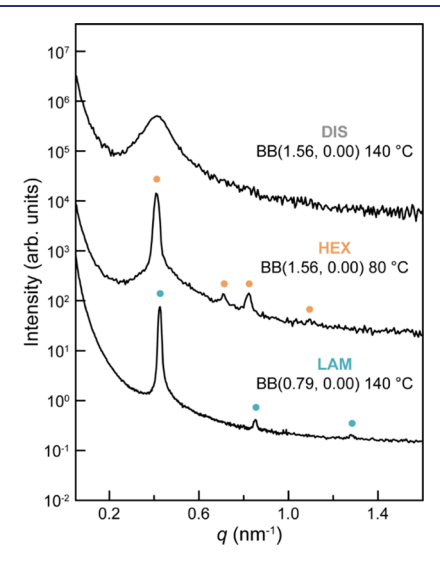


Figure 3. SAXS patterns of representative PEP-PS diblock bottlebrush copolymers. The patterns for BB(0.79, 0.00) and BB(1.56, 0.00) were obtained at the APS and on the Ganesha, respectively.

SAXS patterns of samples with LAM, HEX, and disordered (DIS) phases. An order–disorder transition occurs with sample BB(1.56, 0.00) between 80 and 140 $^{\circ}$ C as evidenced by the loss of higher order reflections and broadening of the principal scattering peak.

The phase portrait for PEP-PS diblocks was then constructed based on a full complement of SAXS patterns (see Figure S9). The ordinate of the diagram is N/T, which is proportional to χN where χ ($\sim T^{-1}$) is the Flory–Huggins interaction parameter. Here, T is the temperature in Kelvin, and N denotes the volumetric degree of polymerization, defined by

$$N = \left(\frac{M_{\rm n}}{\rho_{\rm PEP} f_{\rm PEP} + \rho_{\rm PS} f_{\rm PS}}\right) \frac{1}{N_{\rm av} v_{\rm ref}} \tag{1}$$

where $M_{\rm n}$ is the number-average MW of the diblock, ρ is the density of the constituent blocks ($\rho_{\rm PEP} = 0.79$ g/mL and $\rho_{\rm PS} = 0.969$ g/mL), f is the volume fraction of each component, $N_{\rm av}$ is Avogadro's constant, and the reference volume $\nu_{\rm ref}$ is chosen as 118 Å³. Figure 4 depicts the resulting phase portrait

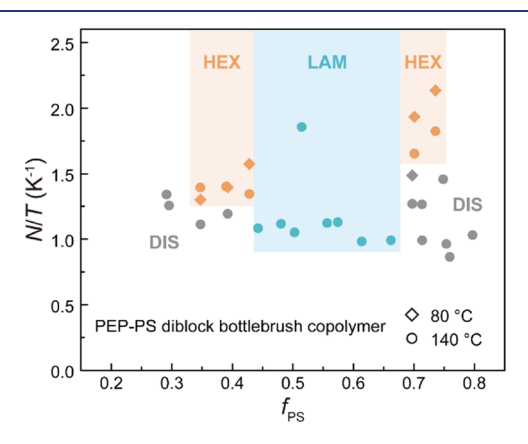


Figure 4. Phase portrait for PEP-PS diblock bottlebrush copolymers. Some samples were measured both at 80 and 140 $^{\circ}$ C.

of the PEP-PS diblock bottle brush copolymers; the molecular parameters are provided in Table S1. The results are qualitatively consistent with previous studies of diblock bottle brush copolymers, 34,42 that is, the sequence of ordered phases HEX-LAM-HEX is observed with increasing $f_{\rm PS}$, whereas HEX-GYR-LAM-GYR-HEX is typically found in linear diblocks. We did not find evidence of any network phase in these PEP-PS bottle brush diblocks.

From Figure 4, the LAM window ranged from $0.43 < f_{PS} <$ 0.68, accompanied by HEX windows on both sides. The LAM window is narrower than that usually found in diblock bottlebrushes, 34,42,43 which can be attributed to the relative flexibility of the bottlebrush copolymers with relatively short (ca. 1 kDa) side chains investigated in this study. 44 An interesting phenomenon is that the ordered phase window is asymmetric with respect to the order-disorder transition (ODT). Specifically, the HEX-to-DIS transition occurs at a critical N/T value that is about 50% higher than that of the adjacent LAM-DIS transition for $f_{PS} \ge 0.7$, which has not been reported in linear diblocks. The same effect is evident on the PS-lean side of the phase map, albeit with a smaller (but still substantial) offset in the critical N/T value. The asymmetric ODT might be rooted in the difference in $\overline{N} = N(b^3/v)^2$ between the PS and PEP side chains, where b and v are the statistical segment length and segment volume, respectively. This will change the space-filling characteristics for the PEP and PS bottlebrush blocks, mimicking the effects of conformational asymmetry in linear diblock copolymers, which is well documented to produce a skewed phase diagram much like that found in Figure 4.16

Phase Behavior of PEP-PS-PEO Triblock Bottlebrush Copolymers. Compared with diblock copolymers, ABC triblock terpolymers have a significantly larger set of molecular parameters (two independent f_i and three distinct χ_{ij} values), enhancing the possibility of obtaining complex phases. In particular, in a pioneering study, Epps and co-workers prepared a large library of linear polyisoprene-PS-PEO (ISO) triblocks and found a large window of network phases that included a core—shell GYR (space group Ia3d), an orthorhombic tricontinuous network (Fddd), and an alternating gyroid

(I4₁32).⁴⁰ Inspired by that work, we introduced a third PEO block and prepared over 100 PEP-PS-PEO triblock bottlebrush copolymers for investigation of phase behavior. The ternary phase portrait of the PEP-PS-PEO copolymers, based on SAXS patterns (representative patterns are presented in Figure S10) supplemented by transmission electron microscopy (TEM) images, is shown in Figure 5. Remarkably, a wide window of

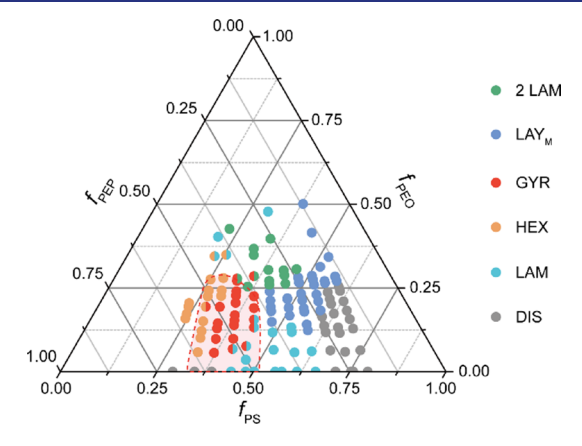


Figure 5. Phase portrait of PEP-PS-PEO triblock bottlebrush copolymers. Samples were measured at 140 $^{\circ}$ C. Here, 2 LAM, LAY_M, GYR, HEX, LAM, and DIS denote two lamellar phases, modulated layer, GYR, hexagonal packed cylinder, lamellae, and DIS phase, respectively. The double-color circles indicate samples with the coexistence of phases indicated by the colors. The current paper focuses on the highlighted region centered around GYR (shaded pink).

network (GYR) bounded by 0.35 < $f_{\rm PEP}$ < 0.58, 0.28 < $f_{\rm PS}$ < 0.45, and 0.05 < $f_{\rm PEO}$ < 0.30 is found in the phase portrait, surrounded by HEX, LAM, and DIS as well as some other intriguing phases. Molecular parameters of the samples in the highlighted composition region are listed in Table 2, and those of other PEP-PS-PEO triblocks are provided in Table S2. The left—right asymmetry of the ordered phase window stems primarily from the expected asymmetrical χ values: $\chi_{\rm PEP-PS} > \chi_{\rm PS-PEO}$ based on linear systems. The focus of this paper is the GYR network. Thus only the highlighted region in Figure 5 will be discussed further. The investigation of other phases will be deferred to a future manuscript.

GYR Phase in PEP-PS-PEO Triblock Bottlebrush Copolymers. This section first describes assignment of the GYR phase illustrated with representative data from sample BB(1.00, 0.23). The SAXS pattern obtained from BB(1.00, 0.23) (Figure 6) displays a good signal-to-noise ratio and excellent q resolution, enabling the indexing of Bragg reflections with the cubic Ia3d space group (Q^{230}) at $q/q^* = \sqrt{6}$, $\sqrt{8}$, $\sqrt{14}$, $\sqrt{16}$, $\sqrt{20}$, $\sqrt{22}$, $\sqrt{24}$, $\sqrt{26}$. Here, $q^* = q_{001} = 2\pi/d_{001}$, where $d_{001} = a$ is the unit cell lattice parameter, and the principal peak corresponds to $q_{211} = \sqrt{6}q^*$. SAXS measurements were conducted at 140 °C to insure against PEO crystallization. Nevertheless, cooling to room temperature did not disrupt the GYR SAXS pattern, although the Bragg peaks did broaden somewhat (Figure S11). The other traces in Figure 6 provide representative examples of SAXS patterns assigned to HEX, LAM, and DIS, as indicated in the figure.

Differential scanning calorimetry (DSC) experiments provided an estimate of PEO block crystallinity in each

Table 2. Molecular Parameters of Gyroid-Forming PEP-PS-PEO Bottlebrush Block Terpolymers

${ m ID}^a$	number ^b	$M_{\rm n} ({\rm kg/mol})^c$	$N_{ m bb}{}^d$	\mathcal{D}^e
BB(1.00, 0.00-0.23)	5	27.2-36.7	21.5-30.3	1.13-1.14
BB(1.08, 0.00-0.08)	3	28.7-31.6	22.7-25.4	1.12-1.13
BB(1.27, 0.00-0.27)	10	27.6-40.2	21.8-33.4	1.12-1.16
BB(1.56, 0.00-0.28)	9	30.1-44.6	23.8-37.0	1.11-1.13
BB(1.86, 0.00-0.28)	9	27.8-41.0	21.9-34.0	1.10-1.12

"Samples with constant $f_{\text{PEP}}/f_{\text{PS}}$ identified as BB($f_{\text{PEP}}/f_{\text{PS}}$, $f_{\text{PEO,min}}-f_{\text{PEO,max}}$), where $f_{\text{PEO,min}}-f_{\text{PEO,max}}$ represents the range of f_{PEO} . "Number of samples in each $f_{\text{PEP}}/f_{\text{PS}}$ family." $f_{\text{PEO,min}}$ of PEP-PS diblocks BB($f_{\text{PEP}}/f_{\text{PS}}$, 0.00) was determined by SEC with an LS detector using a f_{PEO} discontinuity weight average of the $f_{\text{PEP}}/f_{\text{PS}}$ and PS homopolymers, while $f_{\text{PEO,min}}$ of PEP-PS-PEO triblocks BB($f_{\text{PEP}}/f_{\text{PS}}$, f_{PEO}) was calculated by combining the $f_{\text{PEO,min}}$ of the mother diblock and the weight fraction of each component. Backbone degree of polymerization calculated using the volume fraction and MW. Determined by SEC with a RI detector using THF as the eluent.

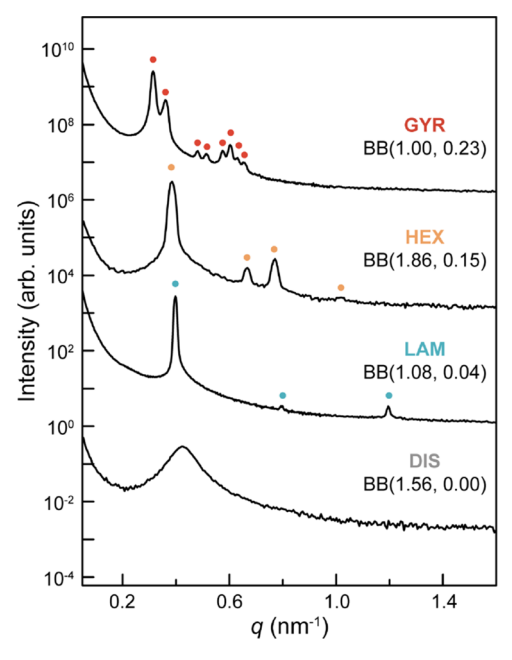


Figure 6. Typical SAXS patterns obtained from PEP-PS-PEO triblock bottlebrush copolymers located in the highlighted region of Figure 5. Samples were measured at 140 °C. BB(1.56, 0.00) and BB(1.86, 0.15) were measured with the Ganesha instrument, whereas the data for BB(1.08, 0.04) and BB(1.00, 0.23) were obtained at the APS. Points situated above the diffraction peaks identify the allowed reflections for the assigned phase.

bottlebrush, which affords strong evidence for the segregation of PEO and PS blocks. Integration of the endothermic peaks in DSC traces (Figure S12), followed by normalization by the PEO weight fraction and the heat of fusion for PEO crystals (213 J/g), ⁴⁰ yielded the degree of PEO crystallinity. The results of samples along the BB(1.56, $f_{\rm PEO}$) isopleth are presented in Figure 7. The GYR phase survives when the PEO crystallinity approaches a high limiting value (>30%), indicative of the PEO block segregating from the PS block, at least for the GYR samples with the highest PEO compositions.

Figure 8A depicts the GYR SAXS patterns of samples along the BB(1.27, $f_{\rm PEO}$) isopleth. For each SAXS pattern in Figure 8A, eight characteristic peaks associated with Q²³⁰ were exactly identified. The presence of a small bump near the principal peak in samples with relatively high $f_{\rm PEO}$ ($f_{\rm PEO}=0.24$ and 0.27) suggests the possible presence of another minor phase. With the increase in $f_{\rm PEO}$, the Q²³⁰ peaks with similar relative intensities shift consistently to lower q. The unit cell dimensions calculated from the SAXS patterns (d_{001}) are

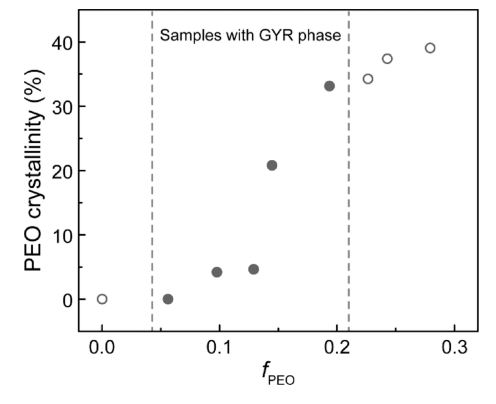


Figure 7. PEO crystallinity of bottlebrush copolymers along the BB(1.56, f_{PEO}) isopleth.

presented in Figure 8B as a function of backbone degree of polymerization $(N_{\rm bb})$ in double logarithmic format. The results range from ~39 to ~53 nm (limited by the modest $N_{\rm bb}$ of the bottlebrushes), scaling as $d_{001} \sim N_{\rm bb}^{0.92\pm0.03}$ ($R^2=0.99$). The continuous evolution of d_{001} with $N_{\rm bb}$ not only suggests a universal morphology for all GYR samples, that is, a core—shell GYR, but also indicates excellent control over the unit cell dimensions by the synthesis procedure. The strong dependence on chain length, which exceeds the strong-segregation-limit expectation of $N^{2/3}$, holds promise for achieving significantly larger unit cells and accessing the photonic regime.

TEM was employed to image the GYR morphology directly. Ultrathin sections (<100 nm) obtained by cryo-microtoming at -70 °C were stained with freshly prepared RuO₄ solutions, which preferentially reacts with the PS and PEO domains (gray regions in TEM images) leaving the PEP domains unstained (white regions). While long-range order was not obtained, images consistent with a 3D network structure were recorded (Figure S13). We attribute the absence of a long-range order to breakout crystallization of the PEO blocks (see the Supporting Information), exacerbated by the soft, continuous, and lowglass transition temperature PEP matrix ($T_{\rm g,PEP} \approx -60$ °C) and brittle PS domains. Based on the SAXS and DSC results, along with the composition of the triblock bottlebrush polymer, we conclude that the Q²³⁰ morphology in this study corresponds to a core–shell GYR, a three-color analogue to the two-color GYR in diblock copolymers.⁴⁸ (Here we note that a previous study with linear PS-PI-PS-PEO tetrablock terpolymers documents a correlation between PEO crystallinity measured by DSC and microdomain segregation.⁴⁹) Additionally, the GYR phase appears to be thermodynamically stable based on consistent results obtained with thermal annealing and solvent casting (Figure S14). This is therefore the first time a GYR

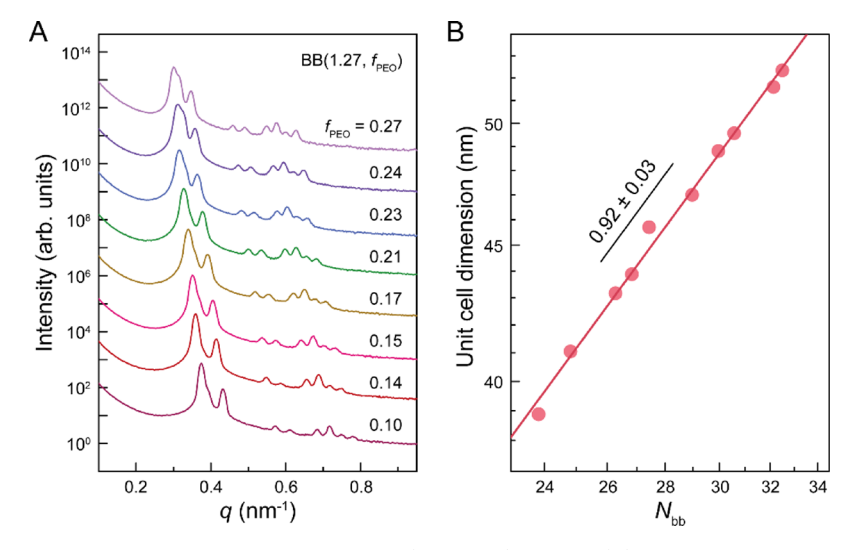


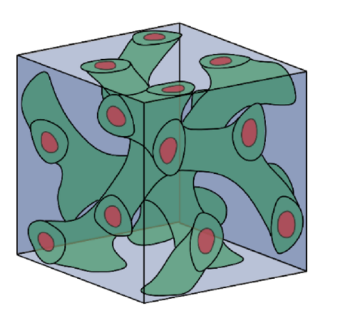
Figure 8. SAXS patterns of samples with the GYR phase along the BB(1.27, f_{PEO}) isopleth (A) and the calculated gyroid unit cell dimension (B). Samples were measured at 140 °C. Two points with the smallest and largest N_{bb} in (B) are from samples with other phases coexisting with gyroid (patterns are not shown in (A)). The axes in (B) are on logarithmic scales. The scaling exponent of the unit cell dimension with N_{bb} is 0.92 ± 0.03 ($R^2 = 0.99$).

network phase has been achieved in bottlebrush block polymers.

DISCUSSION

In this study, we synthesized 133 bottlebrush copolymers by ROMP to systematically explore the phase behavior of both PEP-PS diblock and PEP-PS-PEO triblock bottlebrush block polymers. The combination of anionic polymerization and ROMP of norbornene-functionalized macromonomers endows the final polymers with highly controllable architecture, $M_{\rm n}$, and compositions as well as narrow dispersity, generating accurate models for morphological investigation (Figure 2). The morphological results of the PEP-PS diblocks are consistent with previous studies, 34,42 that is, no network phases appear (Figure 4). The introduction of a third PEO block opens a relatively wide GYR window (Figure 5); for the first time a network phase has been achieved in bottlebrush block polymers. We anticipate a gradual and continuous increase in the segregation between the PS and PEO blocks as f_{PEO} increases. Substantial crystallization of PEO for f_{PEO} > 0.14 (Figure 7) obtained from DSC measurements (Figure S12) is consistent with discrete domains of PEO embedded within PS. Less segregation is evident at lower PEO content. However, once the GYR phase forms there is a continuous increase in the unit cell dimensions with $N_{\rm bb}$ (Figure 8), associated with a core-shell GYR morphology, where parallel PEP/PS and PS/PEO interfaces enclose the PEO domain, as illustrated in Figure 9.

Prior SCFT calculations suggest that a stable GYR window exists in diblock bottlebrush copolymers, even for architecturally symmetric block bottlebrushes, contradicting experimental results. A possible reason is that the mean-field treatment in SCFT is limited in its ability to describe the strongly stretched backbone conformation and radially stretched side chains, that is, the true degree of backbone stiffening is underestimated. Further shortening the side chain might lead to a GYR phase, but the polymer might no longer meet the bottlebrush definition and the advantage of large unit cell dimensions in block bottlebrushes would be lost. An asymmetric architecture might also increase the tendency to form the GYR phase. The



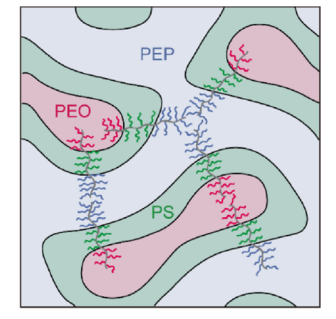


Figure 9. Unit cell of the core—shell GYR (left) and a 2D projection of a cross-section of the morphology (right). Sketches of PEP-PS-PEO chains show how the morphology is assembled.

GYR phase has recently been realized in many linear-bottlebrush copolymers, 35,36 an extreme case of bottlebrush copolymers with asymmetric architectures.

Motivated by previous findings with linear PI-PS-PEO (ISO) triblock polymers, 40 we added variable-length PEO bottlebrush blocks to various PEP-PS bottlebrush diblocks in the search of network phases. Surprisingly, whereas the bottlebrush diblocks produced only LAM and HEX ordered phases (Figure 4), adding a PEO bottlebrush block led to the GYR (Q²³⁰) phase at compositions similar to where this coreshell morphology occurs with ISO (Figure 5). The three χ parameters associated with PEP-PS-PEO bottlebrushes are estimated to be $\chi_{\text{PEP-PS}} = 0.069$, $\chi_{\text{PS-PEO}} = 0.049$, $\chi_{\text{PS-PEO}} = 0.049$, and $\chi_{\text{PEP-PEO}} = 0.157^{50}$ based on linear chains (140 °C), satisfying the definition of non-frustration, $\chi_{\text{PEP-PEO}} > \chi_{\text{PEP-PS}} \approx \chi_{\text{PS-PEO}}$. For non-frustrated ISO block polymers, Epps et al. explored a large composition space and found three networks, Q²³⁰, O⁷⁰, and Q^{214,40} In contrast, we did not find the alternating GYR (Q^{214}) or single network O^{70} phases in the PEP-PS-PEO bottlebrushes (Figure 5) at the analogous compositions. We ascribe this phenomenon to the effect of the "stretched bridging block." Each network phase, Q²³⁰, O⁷⁰, or Q²¹⁴ involves 3D networks separated by a matrix domain, which is either PEP (for PEP-PS-PEO) or PI (for ISO) for Q²³⁰, but a PS midblock domain for both O⁷⁰ and Q²¹⁴. Considering the

block sequence, the PS block acts as a bridge linking the two networks in Q^{214} , whereas PS spans the space between the matrix and network core in Q^{230} and O^{70} (Figure 9). Prior SCFT studies demonstrated that stretched bridging blocks destabilize network phases. Therefore, the more stretched PS block in bottlebrushes apparently results in the absence of the O^{70} and O^{214} phases.

From the ternary phase portrait (Figure 5), the effective f_{PEO} for GYR is as low as 0.06, corresponding to about 1.8 PEO side chains per bottlebrush, and as high as 0.29 which translates to 12 side chains per PEO block. The minority PEO block destabilizes the original phases of the PEP-PS diblock bottlebrushes, leading to the spontaneous formation of the GYR phase with saddle surface interfaces. Compared with the analogous linear ISO system, 40 the stretched bottlebrushes achieve larger GYR unit cell dimensions (53 nm vs 47 nm) with a much shorter contour length (21 nm vs 101 nm). Although relatively modest GYR dimensions have been documented here, increasing $N_{\rm bb}$ should provide access to much larger length scales based on the near linear scaling, d_{001} $\sim N_{
m bb}^{0.92\pm0.03}$ (Figure 8), augmented by the rapid self-assembly kinetics associated with the absence of entanglements afforded by the bottlebrush molecular architecture. Increasing $N_{\rm bh}$ also increases the segregation strength, which should reinforce the extended chain conformations associated with the large scaling exponent found in Figure 8B, providing access to significantly larger unit cell dimensions. The GYR phase in PEP-PS-PEO bottlebrushes is a core-shell GYR (Figure 9). Furthermore, the core-shell GYR in this study is promising for various applications. For example, the PEO domain can dissolve lithium salts,⁵⁴ and such doped GYR materials can be used as solid electrolytes for lithium-ion batteries. Also, the network skeleton in a chemically degradable version of GYR could be selectively etched to produce a porous membrane for separation purposes.

CONCLUSIONS

In this study, 133 bottlebrush block copolymers including PEP-PS diblocks and PEP-PS-PEO triblocks were successfully synthesized by ROMP. The bulk morphologies were characterized by several techniques, most notably SAXS. Only LAM and HEX ordered phases were found in the diblocks, consistent with previous experimental studies but not with SCFT calculations. The contradiction between experiment and theory likely derives from the underestimation of chain stiffening and space-filling in the mean-field SCFT treatment. Introduction of a minority third block resulted in the formation of a core-shell gyroid morphology, the first example of a network phase in bottlebrush block copolymers. Furthermore, the domain size of the GYR scales almost linearly with molecular weight, holding promise for accessing photonic materials by this strategy. This work establishes both similarities and differences in the phase behavior of ABC bottlebrushes and the linear ABC counterparts and paves the way to generating ordered networks with previously unattainably large unit cell dimensions owing to the intrinsic stiffness of the bottlebrush blocks. Discovery of the gyroid network phase also should motivate development of new theoretical approaches capable of accurately treating finite molecular weight bottlebrush molecular architectures.

ASSOCIATED CONTENT

Solution Supporting Information

The Supporting Information is available free of charge at https://pubs.acs.org/doi/10.1021/jacs.2c09674.

Detailed synthesized route, ¹H NMR spectra, SEC traces, molecular parameters, DSC traces, SAXS patterns, and TEM images (PDF)

AUTHOR INFORMATION

Corresponding Authors

Frank S. Bates – Department of Chemical Engineering and Materials Science, University of Minnesota, Minneapolis, Minnesota 55455, United States; orcid.org/0000-0003-3977-1278; Email: bates001@umn.edu

Timothy P. Lodge — Department of Chemistry and Department of Chemical Engineering and Materials Science, University of Minnesota, Minneapolis, Minnesota 55455, United States; orcid.org/0000-0001-5916-8834; Email: lodge@umn.edu

Authors

Shuquan Cui — Department of Chemistry, University of Minnesota, Minneapolis, Minnesota 55455, United States

Bo Zhang — Department of Chemical Engineering and Materials Science, University of Minnesota, Minneapolis, Minnesota 55455, United States; orcid.org/0000-0001-5366-1855

Liyang Shen – Department of Chemical Engineering and Materials Science, University of Minnesota, Minneapolis, Minnesota 55455, United States; orcid.org/0000-0001-9928-2877

Complete contact information is available at: https://pubs.acs.org/10.1021/jacs.2c09674

Notes

The authors declare no competing financial interest.

ACKNOWLEDGMENTS

This work was supported by the National Science Foundation (NSF) through the University of Minnesota MRSEC under Award DMR-2011401. Parts of this work were carried out in the Characterization Facility, University of Minnesota, which receives partial support from NSF through the MRSEC program. Synchrotron SAXS experiments were performed at the 12-ID-B beamlines of the Advanced Photon Source (APS). This research used resources of the Advanced Photon Source, a U.S. Department of Energy (DOE) Office of Science User Facility operated for the DOE Office of Science by Argonne National Laboratory under contract no. DE-AC02-06CH11357. We thank Prof. Mahesh Mahanthappa for fruitful discussions and Dr. Qiming He for help with the esterification reaction.

REFERENCES

- (1) Hsueh, H. Y.; Yao, C. T.; Ho, R. M. Well-ordered nanohybrids and nanoporous materials from gyroid block copolymer templates. *Chem. Soc. Rev.* **2015**, *44*, 1974–2018.
- (2) Han, L.; Che, S. A. An overview of materials with triply periodic minimal surfaces and related geometry: from biological structures to self-assembled systems. *Adv. Mater.* **2018**, *30*, No. 1705708.
- (3) Ichikawa, T.; Kato, T.; Ohno, H. 3D continuous water nanosheet as a gyroid minimal surface formed by bicontinuous cubic liquid-crystalline zwitterions. *J. Am. Chem. Soc.* **2012**, *134*, 11354–11357.

- (4) Park, S.; Kim, Y.; Ahn, H.; Kim, J. H.; Yoo, P. J.; Ryu, D. Y. Giant gyroid and templates from high-molecular-weight block copolymer self-assembly. *Sci. Rep.* **2016**, *6*, 36326.
- (5) Barriga, H. M. G.; Holme, M. N.; Stevens, M. M. Cubosomes: the next generation of smart lipid nanoparticles? *Angew. Chem., Int. Ed.* **2019**, *58*, 2958–2978.
- (6) Chan, V. Z. H.; Hoffman, J.; Lee, V. Y.; Iatrou, H.; Avgeropoulos, A.; Hadjichristidis, N.; Miller, R. D.; Thomas, E. L. Ordered bicontinuous nanoporous and nanorelief ceramic films from self assembling polymer precursors. *Science* **1999**, *286*, 1716–1719.
- (7) Robbins, S. W.; Beaucage, P. A.; Sai, H.; Tan, K. W.; Werner, J. G.; Sethna, J. P.; DiSalvo, F. J.; Gruner, S. M.; Van Dover, R. B.; Wiesner, U. Block copolymer self-assembly-directed synthesis of mesoporous gyroidal superconductors. *Sci. Adv.* **2016**, 2, No. e1501119.
- (8) Yang, K. C.; Yao, C. T.; Huang, L. Y.; Tsai, J. C.; Hung, W. S.; Hsueh, H. Y.; Ho, R. M. Single gyroid-structured metallic nanoporous spheres fabricated from double gyroid-forming block copolymers via templated electroless plating. NPG Asia Mater. 2019, 11, 9.
- (9) Turner, M. D.; Saba, M.; Zhang, Q. M.; Cumming, B. P.; Schroder-Turk, G. E.; Gu, M. Miniature chiral beamsplitter based on gyroid photonic crystals. *Nat. Photonics* **2013**, *7*, 801–805.
- (10) Cote, B. M.; Lenart, W. R.; Ellison, C. J.; Ferry, V. E. Surface structure dependent circular dichroism in single and double gyroid metamaterials. *Adv. Opt. Mater.* **2022**, *10*, No. 2200363.
- (11) Bates, F. S. Polymer-polymer phase-behavior. *Science* **1991**, 251, 898–905.
- (12) Bates, C. M.; Bates, F. S. 50th anniversary perspective: block polymers-pure potential. *Macromolecules* **2017**, *50*, 3–22.
- (13) Leibler, L. Theory of microphase separation in block copolymers. *Macromolecules* **1980**, *13*, 1602–1617.
- (14) Bates, F. S.; Fredrickson, G. H. Block copolymers designer soft materials. *Phys. Today* **1999**, *52*, 32–38.
- (15) Lodge, T. P. Block copolymers: long-term growth with added value. *Macromolecules* **2020**, *53*, 2–4.
- (16) Abetz, V.; Simon, P. F. W. Phase behaviour and morphologies of block copolymers. *Adv. Polym. Sci.* **2005**, *189*, 125–212.
- (17) Meuler, A. J.; Hillmyer, M. A.; Bates, F. S. Ordered network mesostructures in block polymer materials. *Macromolecules* **2009**, *42*, 7221–7250.
- (18) Runge, M. B.; Bowden, N. B. Synthesis of high molecular weight comb block copolymers and their assembly into ordered morphologies in the solid state. *J. Am. Chem. Soc.* **2007**, *129*, 10551–10560.
- (19) Runge, M. B.; Lipscomb, C. E.; Ditzler, L. R.; Mahanthappa, M. K.; Tivanski, A. V.; Bowden, N. B. Investigation of the assembly of comb block copolymers in the solid state. *Macromolecules* **2008**, *41*, 7687–7694.
- (20) Lin, F. Y.; Hohmann, A. D.; Hernandez, N.; Shen, L. Y.; Dietrich, H.; Cochran, E. W. Self-assembly of poly(styrene-block-acrylated epoxidized soybean oil) star-brush-like block copolymers. *Macromolecules* **2020**, *53*, 8095–8107.
- (21) Sveinbjornsson, B. R.; Weitekamp, R. A.; Miyake, G. M.; Xia, Y.; Atwater, H. A.; Grubbs, R. H. Rapid self-assembly of brush block copolymers to photonic crystals. *Proc. Natl. Acad. Sci. U. S. A.* **2012**, 109, 14332–14336.
- (22) Matsen, M. W. The standard Gaussian model for block copolymer melts. J. Phys.: Condens. Matter 2002, 14, R21–R47.
- (23) Verduzco, R.; Li, X. Y.; Peseka, S. L.; Steinc, G. E. Structure, function, self-assembly, and applications of bottlebrush copolymers. *Chem. Soc. Rev.* **2015**, *44*, 2405–2420.
- (24) Nguyen, H. V. T.; Jiang, Y.; Mohapatra, S.; Wang, W. C.; Barnes, J. C.; Oldenhuis, N. J.; Chen, K. K.; Axelrod, S.; Huang, Z. H.; Chen, Q. X.; Golder, M. R.; Young, K.; Suvlu, D.; Shen, Y. Z.; Willard, A. P.; Hore, M. J. A.; Gomez-Bombarelli, R.; Johnson, J. A. Bottlebrush polymers with flexible enantiomeric side chains display differential biological properties. *Nat. Chem.* **2022**, *14*, 85–93.
- (25) Daniel, W. F. M.; Burdynska, J.; Vatankhah-Varnoosfaderani, M.; Matyjaszewski, K.; Paturej, J.; Rubinstein, M.; Dobrynin, A. V.;

- Sheiko, S. S. Solvent-free, supersoft and superelastic bottlebrush melts and networks. *Nat. Mater.* **2016**, *15*, 183–189.
- (26) Dalsin, S. J.; Rions-Maehren, T. G.; Beam, M. D.; Bates, F. S.; Hillmyer, M. A.; Matsen, M. W. Bottlebrush block polymers: quantitative theory and experiments. *ACS Nano* **2015**, *9*, 12233—12245.
- (27) Xia, Y.; Olsen, B. D.; Kornfield, J. A.; Grubbs, R. H. Efficient synthesis of narrowly dispersed brush copolymers and study of their assemblies: the importance of side-chain arrangement. *J. Am. Chem. Soc.* **2009**, *131*, 18525–18532.
- (28) Miyake, G. M.; Weitekamp, R. A.; Piunova, V. A.; Grubbs, R. H. Synthesis of isocyanate-based brush block copolymers and their rapid self-assembly to infrared-reflecting photonic crystals. *J. Am. Chem. Soc.* **2012**, *134*, 14249–14254.
- (29) Rzayev, J. Synthesis of polystyrene-polylactide bottlebrush block copolymers and their melt self-assembly into large domain nanostructures. *Macromolecules* **2009**, 42, 2135–2141.
- (30) Bolton, J.; Bailey, T. S.; Rzayev, J. Large pore size nanoporous materials from the self-assembly of asymmetric bottlebrush block copolymers. *Nano Lett.* **2011**, *11*, 998–1001.
- (31) Park, S. J.; Cheong, G. K.; Bates, F. S.; Dorfman, K. D. Stability of the double gyroid phase in bottlebrush diblock copolymer melts. *Macromolecules* **2021**, *54*, 9063–9070.
- (32) Lequieu, J.; Quah, T.; Delaney, K. T.; Fredrickson, G. H. Complete photonic band gaps with nonfrustrated ABC bottlebrush block polymers. *ACS Macro Lett.* **2020**, *9*, 1074–1080.
- (33) Kawamoto, K.; Zhong, M. J.; Gadelrab, K. R.; Cheng, L. C.; Ross, C. A.; Alexander-Katz, A.; Johnson, J. A. Graft-through synthesis and assembly of Janus bottlebrush polymers from A-branch-B diblock macromonomers. *J. Am. Chem. Soc.* **2016**, *138*, 11501–11504.
- (34) Jiang, L. Y.; Nykypanchuk, D.; Pastore, V. J.; Rzayev, J. Morphological behavior of compositionally gradient polystyrene-polylactide bottlebrush copolymers. *Macromolecules* **2019**, *52*, 8217–8226.
- (35) Liberman, L.; Coughlin, M. L.; Weigand, S.; Bates, F. S.; Lodge, T. P. Phase behavior of linear-bottlebrush block polymers. *Macromolecules* **2022**, *55*, 2821–2831.
- (36) Liberman, L.; Coughlin, M. L.; Weigand, S.; Edmund, J.; Bates, F. S.; Lodge, T. P. Impact of side-chain length on the self-assembly of linear-bottlebrush diblock copolymers. *Macromolecules* **2022**, *55*, 4947–4955.
- (37) Matsen, M. W.; Bates, F. S. Unifying weak- and strong-segregation block copolymer theories. *Macromolecules* **1996**, 29, 1091–1098.
- (38) Love, J. A.; Morgan, J. P.; Trnka, T. M.; Grubbs, R. H. A practical and highly active ruthenium-based catalyst that effects the cross metathesis of acrylonitrile. *Angew. Chem., Int. Ed.* **2002**, *41*, 4035–4037.
- (39) Lin, T. P.; Chang, A. B.; Chen, H. Y.; Liberman-Martin, A. L.; Bates, C. M.; Voegtle, M. J.; Bauer, C. A.; Grubbs, R. H. Control of grafting density and distribution in graft polymers by living ring-opening metathesis copolymerization. *J. Am. Chem. Soc.* **2017**, *139*, 3896–3903.
- (40) Epps, T. H.; Cochran, E. W.; Bailey, T. S.; Waletzko, R. S.; Hardy, C. M.; Bates, F. S. Ordered network phases in linear poly(isoprene-b-styrene-b-ethylene oxide) triblock copolymers. *Macromolecules* **2004**, *37*, 8325–8341.
- (41) Lindsay, A. P.; Jayaraman, A.; Peterson, A. J.; Mueller, A. J.; Weigand, S.; Almdal, K.; Mahanthappa, M. K.; Lodge, T. P.; Bates, F. S. Reevaluation of poly(ethylene-alt-propylene)-block-polydimethylsiloxane phase behavior uncovers topological close-packing and epitaxial quasicrystal growth. *ACS Nano* **2021**, *15*, 9453–9468.
- (42) Gai, Y.; Song, D. P.; Yavitt, B. M.; Watkins, J. J. Polystyrene-block-poly(ethylene oxide) bottlebrush block copolymer morphology transitions: influence of side chain length and volume fraction. *Macromolecules* **2017**, *50*, 1503–1511.
- (43) Choo, Y.; Mahajan, L. H.; Gopinadhan, M.; Ndaya, D.; Deshmukh, P.; Kasi, R. M.; Osuji, C. O. Phase behavior of

polylactide-based liquid crystalline brushlike block copolymers. *Macromolecules* **2015**, 48, 8315–8322.

- (44) Chremos, A.; Theodorakis, P. E. Impact of intrinsic backbone chain stiffness on the morphologies of bottle-brush diblock copolymers. *Polymer* **2016**, *97*, 191–195.
- (45) Chang, A. B.; Bates, F. S. The ABCs of block polymers. *Macromolecules* **2020**, 53, 2765–2768.
- (46) Sakurai, S.; Hashimoto, T.; Fetters, L. J. Morphology of polystyrene-block-poly(ethylene-alt-propylene) diblock copolymers in the strong-segregation limit. *Macromolecules* **1995**, *28*, 7947–7949.
- (47) Cochran, E. W.; Morse, D. C.; Bates, F. S. Design of ABC triblock copolymers near the ODT with the random phase approximation. *Macromolecules* **2003**, *36*, 782–792.
- (48) Shefelbine, T. A.; Vigild, M. E.; Matsen, M. W.; Hajduk, D. A.; Hillmyer, M. A.; Cussler, E. L.; Bates, F. S. Core-shell gyroid morphology in a poly(isoprene-block-styrene-block-dimethylsiloxane) triblock copolymer. *J. Am. Chem. Soc.* **1999**, *121*, 8457–8465.
- (49) Zhang, J. W.; Sides, S.; Bates, F. S. Ordering of sphere forming SISO tetrablock terpolymers on a simple hexagonal lattice. *Macromolecules* **2012**, *45*, 256–265.
- (50) Xie, S. Y.; Lodge, T. P. Phase behavior of binary polymer blends doped with salt. *Macromolecules* **2018**, *51*, 266–274.
- (51) Xie, Q.; Qjang, Y. C.; Li, W. H. Regulate the stability of gyroids of ABC-type multiblock copolymers by controlling the packing frustration. *ACS Macro Lett.* **2020**, *9*, 278–283.
- (52) Xie, Q.; Qiang, Y. C.; Li, W. H. Single gyroid self-assembled by linear BABAB pentablock copolymer. *ACS Macro Lett.* **2022**, *11*, 205–209.
- (53) Gu, W. Y.; Huh, J.; Hong, S. W.; Sveinbjornsson, B. R.; Park, C.; Grubbs, R. H.; Russell, T. P. Self-assembly of symmetric brush diblock copolymers. *ACS Nano* **2013**, *7*, 2551–2558.
- (54) Bates, C. M.; Chang, A. B.; Momcilovic, N.; Jones, S. C.; Grubbs, R. H. ABA triblock brush polymers: synthesis, self-assembly, conductivity, and rheological properties. *Macromolecules* **2015**, 48, 4967–4973.

□ Recommended by ACS

Thermoresponsive Modular Nano-Objects Via RAFT Dispersion Polymerization in a Non-Polar Solvent

Gianmaria Gardoni, Davide Moscatelli, et al.

DECEMBER 07, 2022

ACS APPLIED POLYMER MATERIALS

READ 🗹

Non-equilibrium Nanoassemblies Constructed by Confined Coordination on a Polymer Chain

Zhikai Li, Xiaopeng Li, et al.

NOVEMBER 21, 2022

JOURNAL OF THE AMERICAN CHEMICAL SOCIETY

READ 🗹

Efficient Creation and Morphological Analysis of ABC Triblock Terpolymer Libraries

Elizabeth A. Murphy, Craig J. Hawker, et al.

OCTOBER 03, 2022

MACROMOLECULES

READ 🗹

Pyrrole-Containing ABA Triblock Brush Polymers as Dual Functional Molecules to Facilely Access Diverse Mesostructured Materials

Guokang He, Guangtao Li, et al.

OCTOBER 14, 2022

MACROMOLECULES

READ 🗹

Get More Suggestions >